

# Microwave-Activated Controlled-Z Gate for Fixed-Frequency Fluxonium Qubits

Konstantin N. Nesterov,<sup>1</sup> Ivan V. Pechenezhskiy,<sup>2</sup> Chen Wang,<sup>3</sup> Vladimir E. Manucharyan,<sup>2</sup> and Maxim G. Vavilov<sup>1</sup>

<sup>1</sup>*Department of Physics, University of Wisconsin-Madison, Madison, WI 53706*

<sup>2</sup>*Department of Physics, Joint Quantum Institute, and Center for Nanophysics and Advanced Materials, University of Maryland, College Park, MD 20742*

<sup>3</sup>*Department of Physics, University of Massachusetts, Amherst, MA 01003*

(Dated: February 8, 2018)

The superconducting fluxonium circuit is an artificial atom with a strongly anharmonic spectrum: when biased at a half flux quantum, the lowest qubit transition is an order of magnitude smaller in frequency than those to higher levels. Similar to conventional atomic systems, such a frequency separation between the computational and noncomputational subspaces allows independent optimizations of the qubit coherence and two-qubit interactions. Here we describe a controlled-Z gate for two fluxoniums connected either capacitively or inductively, with qubit transitions fixed near 500 MHz. The gate is activated by a microwave drive at a resonance involving the second excited state. We estimate intrinsic gate fidelities over 99.9% with gate times below 100 ns.

The transmon qubit [1] has been largely responsible for the spectacular breakthrough in superconducting quantum information processing over the last decade [2]. This qubit demonstrates long coherence times [3, 4], high-fidelity gates [5], and reliable readout techniques [6–8]. In the transmon, the qubit transition connects the two lowest levels of a weakly anharmonic electromagnetic oscillator formed by shunting a Josephson junction by an external capacitance. Although multi-qubit devices [9–11] with high-fidelity two-qubit gates [4, 12–14] have already been demonstrated, the weak anharmonicity of the transmon presents a substantial challenge in pushing the fidelities higher. Fundamentally, the main issue is that both the qubit memory and interaction with other qubits are done using transitions with nearly identical frequencies and matrix elements. This prevents decoupling of a qubit from its dissipative environment, e.g., due to the dielectric loss, without proportionally increasing the gate time. Furthermore, stronger coupling of two transmons requires a smaller detuning of their frequencies, which in turn enhances the uncontrolled state leakage outside of the computational subspace.

In atomic systems, qubit states are chosen in such a way that the transition between them is forbidden by the selection rules to provide long coherence in the computational subspace. Quantum gates and qubit readout are performed through transitions outside of that subspace with stronger coupling to electromagnetic fields. Such separation of quantum states for information storage and processing allows one to perform many high-fidelity gates before the qubit state is spoiled by decoherence. This was realized in architectures based on nitrogen-vacancy centers [15], trapped ions [16], and Rydberg atoms [17]. In superconducting systems, the idea to separate information storage and processing led to experiments where the qubit quantum state is stored in a high-quality microwave resonator as a single photon [18] or a multi-photon state [19], while the physical superconducting qubits are used only for short times during gate

realizations.

In this paper, we consider the fluxonium superconducting qubit [20–22] biased at a half of magnetic-flux quantum, which can be utilized as both a long memory and a fast processor of quantum information. The fluxonium is topologically distinct from the transmon and thereby combines strong Josephson nonlinearity with complete insensitivity to offset charges [20, 23]. As a result, the fluxonium shares many spectral features with a multi-level atomic system. Its two lowest energy states can have a very long coherence time [21, 24] and thus suit well for quantum information storage. Higher energy states are separated by much larger energy spacings and have large transition matrix elements similar to a typical transmon, which makes them ideal for the information processing [21, 22, 25]. We propose a controlled-Z (CZ) gate for two fluxoniums with an always-on interaction realized through either electrostatic or inductive coupling. The gate is activated by a microwave pulse, while the qubits are kept at fixed frequencies. By numerically simulating the driven dynamics and taking into account excited states, we find that the intrinsic gate fidelity can be above 99.9% for gate times below 100 ns for realistic coupling parameters.

*Fluxonium at half flux-quantum bias* — The fluxonium superconducting circuit [Fig. 1(a)] features a long Josephson-junction array with the total inductance  $L_\alpha$  shunting a phase-slip Josephson junction, where  $\alpha = A$  or  $B$  is a qubit label in a two-qubit device. The circuit is characterized by three energy scales: the charging energy  $E_{C,\alpha} = e^2/2C_\alpha$ , the inductive energy  $E_{L,\alpha} = (\hbar/2e)^2/L_\alpha$ , and the Josephson energy  $E_{J,\alpha}$ , where  $-e$  is the electron charge,  $C_\alpha$  is the total capacitance, and  $\hbar = h/2\pi$  is the Planck constant. With an external flux  $\Phi_{\text{ext},\alpha} = (\hbar/2e)\phi_{\text{ext},\alpha}$  threading the loop formed by the Josephson junction and the inductance, the Hamiltonian of fluxonium  $\alpha$  is [20]

$$\hat{H}_\alpha^{(0)} = 4E_{C,\alpha}\hat{n}_\alpha^2 + \frac{1}{2}E_{L,\alpha}\hat{\varphi}_\alpha^2 - E_{J,\alpha}\cos(\hat{\varphi}_\alpha - \phi_{\text{ext},\alpha}). \quad (1)$$

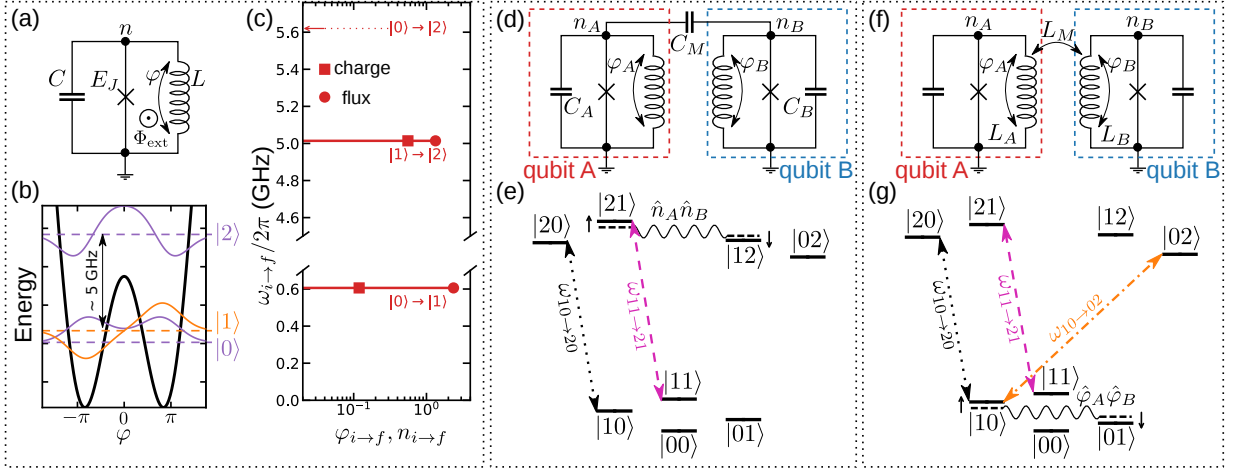


FIG. 1. (Color online) Left panel: (a) Circuit diagram of a single fluxonium qubit and (b) its lowest three energy levels (dashed lines) and wave functions (thin solid lines) at the flux sweet spot  $\Phi_{\text{ext}} = h/4e$ ; the phase-dependent potential energy is shown by the thick solid line. (c) The horizontal bars represent magnitudes of the charge (squares) and flux (circles) matrix elements for transitions between the three lowest energy states at frequencies  $\omega_{i \rightarrow f}/2\pi$  for parameters of qubit A (see text). The transition  $|0\rangle \rightarrow |2\rangle$  is forbidden,  $\varphi_{0 \rightarrow 2} = n_{0 \rightarrow 2} = 0$ . Middle panel: (d) The circuit diagram of two fluxoniums coupled by a capacitor  $C_M$ . (e) The energy spectrum diagram represents location of its energy levels in the presence of interaction (horizontal solid lines). The primary effect of interaction is to induce the level repulsion (marked by vertical arrows) of states  $|12\rangle_0$  and  $|21\rangle_0$  without coupling (horizontal dashed lines). The repulsion results in  $\omega_{10 \rightarrow 20} \neq \omega_{11 \rightarrow 21}$  and the gate is realized by a resonant drive of the  $|11\rangle \rightarrow |21\rangle$  transition. Right panel: Two fluxoniums coupled by a common inductance  $L_M$ ; the notation follows panels (d) and (e). The flux-flux interaction  $\hat{\varphi}_A \hat{\varphi}_B$  primarily affects states  $|10\rangle$  and  $|01\rangle$ , leads to  $\omega_{10 \rightarrow 20} \neq \omega_{11 \rightarrow 21}$ , and permits the  $|10\rangle \rightarrow |02\rangle$  transition (dash-dotted line).

Here,  $\hat{\varphi}_\alpha$  and  $\hat{n}_\alpha$  are the generalized flux and charge (Cooper-pair number) operators satisfying  $[\hat{\varphi}_\alpha, \hat{n}_\alpha] = i$ . There is a wide and experimentally-attainable parameter space suitable for the proposed CZ gate. For illustration purposes, we use the following parameters:  $E_{C,A}/h = 1.5$  GHz,  $E_{C,B}/h = 1.2$  GHz,  $E_{J,A}/h = 5.5$  GHz,  $E_{J,B}/h = 5.7$  GHz, and  $E_{L,A}/h = E_{L,B}/h = 1$  GHz. Unlike in transmons,  $E_{J,\alpha}/E_{C,\alpha}$  is not required to be large because the fluxonium is insensitive to the charge noise [23].

When biased at one half of magnetic flux quantum ( $\varphi_{\text{ext},\alpha} = \pi$ ), the fluxoniums are at their sweet spots with respect to the flux noise [21]. The corresponding potential energy is shown in Fig. 1(b) along with three lowest eigenenergies  $\varepsilon_k^\alpha$  and eigenfunctions  $|k_\alpha\rangle$ . The lowest two levels are used as the qubit computational states. They are the symmetric and antisymmetric combinations of the states localized at the two potential minima. The splitting between them is determined by the tunneling rate between the wells, which gives relatively small  $\omega_{0 \rightarrow 1}^\alpha/2\pi \sim 500$  MHz, where  $\omega_{i \rightarrow f}^\alpha = (\varepsilon_f^\alpha - \varepsilon_i^\alpha)/\hbar$  is the frequency of the  $|i_\alpha\rangle \rightarrow |f_\alpha\rangle$  transition. On the other hand,  $\omega_{1 \rightarrow 2}^\alpha/2\pi \sim 5$  GHz, which facilitates strong coupling and fast gates.

The hierarchies of single-qubit transition frequencies and matrix elements of flux and charge of qubit A are shown in Fig. 1(c). Each fluxonium level has a well-defined even or odd parity with respect to  $\varphi \rightarrow -\varphi$ , implying selection rules for matrix elements, which are

exactly zero for two levels of the same parity [25, 26]. Thus,  $\varphi_{0 \rightarrow 2}^\alpha = n_{0 \rightarrow 2}^\alpha = 0$ , where  $O_{i \rightarrow f}^\alpha = |\langle i_\alpha | \hat{O}_\alpha | f_\alpha \rangle|$  is the magnitude of the single-qubit matrix element ( $\hat{O} = \hat{\varphi}$  or  $\hat{n}$ ). Among the allowed transitions,  $\varphi_{0 \rightarrow 1}^\alpha \gtrsim \varphi_{1 \rightarrow 2}^\alpha$  and  $n_{0 \rightarrow 1}^\alpha \ll n_{1 \rightarrow 2}^\alpha$ , where  $n_{0 \rightarrow 1}^\alpha$  is suppressed due to relatively weak tunneling between the wells. The relation between the charge and flux matrix elements can be found by computing  $[\hat{\varphi}_\alpha, \hat{H}_\alpha^{(0)}]$ , which yields  $\omega_{i \rightarrow f}^\alpha \varphi_{i \rightarrow f}^\alpha = 8E_{C,\alpha} n_{i \rightarrow f}^\alpha$ .

*Capacitive coupling* — First, we consider coupling realized via a capacitor  $C_M$  as shown in Fig. 1(d). The Hamiltonian of the two-qubit system is

$$\hat{H} = \hat{H}_A^{(0)} + \hat{H}_B^{(0)} + \hat{V} + \hat{H}_{\text{drive}}, \quad (2)$$

where  $\hat{V}$  is the qubit-qubit interaction and  $\hat{H}_{\text{drive}}$  describes the external microwave drive. In the limit  $C_M \ll C_A, C_B$ , we have [27]

$$\hat{V} = J_C \hat{n}_A \hat{n}_B \quad \text{with} \quad J_C = 4e^2 C_M / (C_A C_B), \quad (3)$$

where  $\hat{n}_\alpha$  is the total charge on  $C_\alpha$  and the corresponding side of  $C_M$ . We note that  $C_M$  also slightly renormalizes  $E_{C,\alpha}$ . For simplicity, we assume that the drive is directly applied to the qubits:

$$\hat{H}_{\text{drive}} = f(t) \cos(\omega_d t) (\eta_A \hat{n}_A + \eta_B \hat{n}_B). \quad (4)$$

Here  $f(t)$  describes a shape of the microwave pulse, and  $\eta_{A,B}$  are the effective strengths of qubit couplings to the microwave field.

We use the notation  $|kl\rangle$  for an eigenstate of  $\hat{H}$  with  $\hat{H}_{\text{drive}} = 0$ , which is adiabatically connected to the non-interacting eigenstate  $|kl\rangle_0 = |k_A\rangle|l_B\rangle$ . We extend the notation  $n_{i \rightarrow f}^\alpha$  to two-qubit transitions, where  $|i\rangle = |kl\rangle$  and  $|f\rangle = |k'l'\rangle$ , and write  $\omega_{kl \rightarrow k'l'}$  for the frequencies of such transitions.

The main idea of the CZ gate is as follows. When  $\hat{V} = 0$ ,  $\omega_{10 \rightarrow 20} = \omega_{11 \rightarrow 21} = \omega_{1 \rightarrow 2}$ . The interaction  $\hat{V}$  lifts this degeneracy, and the gate can be realized by selectively driving Rabi oscillations between states  $|11\rangle$  and  $|21\rangle$ , see Fig. 1(e). State  $|11\rangle$  accumulates an extra phase factor of  $e^{i\pi}$  after the system completes one oscillation. Therefore, for the ideal pulse shape  $f(t)$ , when other transitions, in particular,  $|10\rangle \rightarrow |20\rangle$ , are not affected, the computational subspace  $\{|00\rangle, |01\rangle, |10\rangle, |11\rangle\}$  would evolve according to the CZ gate operator  $\hat{U}_{\text{CZ}} = \text{diag}(1, 1, 1, -1)$  up to single-qubit Z gates [28].

The hierarchy of single-qubit  $n_{i \rightarrow f}^\alpha$  [Fig. 1(c)] has two important consequences: (i)  $\hat{H}_{\text{drive}}$  couples stronger to the  $|1\rangle \rightarrow |2\rangle$  transition than to the  $|0\rangle \rightarrow |1\rangle$ ; (ii)  $\hat{V}$  leads to much stronger hybridization (level repulsion) between noncomputational states  $|21\rangle$  and  $|12\rangle$  [Fig. 1(e)] than computational ones because  $n_{1 \rightarrow 2}^A n_{1 \rightarrow 2}^B \gg n_{0 \rightarrow 1}^A n_{0 \rightarrow 1}^B$ . As a result, the second-order correction to the energy of state  $|21\rangle$  is by a factor of several hundreds larger than those to the energies of states  $|10\rangle$  and  $|11\rangle$ . Since  $n_{0 \rightarrow 2}^\alpha = n_{2 \rightarrow 0}^\alpha = 0$ , the state  $|20\rangle_0$  does not acquire the perturbative shift from nearby levels  $|02\rangle_0$ ,  $|21\rangle_0$ , and  $|12\rangle_0$ , making  $\omega_{11 \rightarrow 21} \neq \omega_{10 \rightarrow 20}$ .

The gate rate [29], characterized by the frequency mismatch  $\Delta\omega = \omega_{11 \rightarrow 21} - \omega_{10 \rightarrow 20}$ , increases with decreasing  $\delta = |\omega_{1 \rightarrow 2}^A - \omega_{1 \rightarrow 2}^B|$ , which is 248 MHz for our choice of parameters. In general, smaller  $\delta$  leads to faster and better performing gates. Our conservative choice of  $\delta \sim 250$  MHz is motivated by device fabrication uncertainty in a physical implementation of the CZ gate. We numerically diagonalize the two-qubit Hamiltonian (2) at  $\hat{H}_{\text{drive}} = 0$  and study  $\Delta\omega$  and  $n_{kl \rightarrow k'l'}^\alpha$  as a function of the interaction strength  $J_C$ , see Figs. 2(a) and (b). As expected,  $\Delta\omega$  increases monotonically with increasing  $J_C$  [solid line in Fig. 2(a)]. We notice that  $\Delta\omega$  increases much faster than  $\Delta_c = \omega_{00 \rightarrow 01} - \omega_{10 \rightarrow 11}$ , the phase accumulation rate in the computational subspace. The on-off ratio of the CZ gate  $\Delta\omega/\Delta_c \approx 100$  for our parameters.

The matrix elements panel [Fig. 2(b)] illustrates strong mixing between  $|12\rangle_0$  and  $|21\rangle_0$ . While  $n_{10 \rightarrow 20}^A \approx n_{1 \rightarrow 2}^A$  at finite  $J_C$ , the value of  $n_{11 \rightarrow 21}^A$  decreases with increasing  $J_C$  since the dressed state  $|21\rangle$  is a superposition of non-interacting states  $|12\rangle_0$  and  $|21\rangle_0$ . For the same reason,  $n_{11 \rightarrow 21}^B \neq 0$  for  $J_C \neq 0$ .

Figure 2(c) facilitates understanding of how much other transitions with frequencies close to  $\omega_{11 \rightarrow 21}$  are activated because of the finite width of the drive spectrum. Since  $n_{11 \rightarrow 21}^B \gg n_{10 \rightarrow 20}^B$ , undesirable activation of  $|10\rangle \rightarrow |20\rangle$  can be suppressed by applying the drive

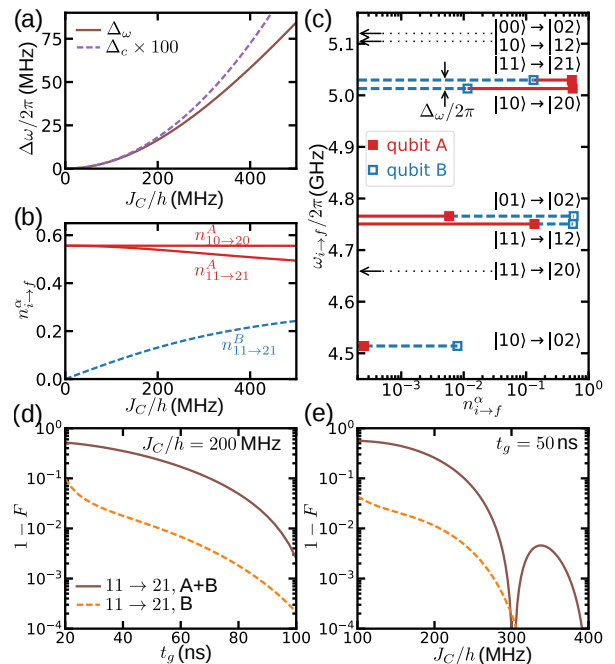


FIG. 2. (Color online) Numerical results for the capacitive coupling. (a) The frequency mismatch  $\Delta\omega$  and the phase accumulation rate  $\Delta_c$  vs the interaction strength  $J_C$ . (b) Amplitudes of the matrix elements of  $\hat{n}_A$  and  $\hat{n}_B$  vs  $J_C$ . (c) Transition frequencies (y-axis) and matrix elements (x-axis) of  $\hat{n}_A$  (filled squares) and  $\hat{n}_B$  (empty squares) at  $J_C/h = 200$  MHz. The transitions without symbols are prohibited by the symmetry. (d, e) The gate error as a function of the gate time  $t_g$  at a fixed  $J_C/h = 200$  MHz (d) and as a function of  $J_C$  at  $t_g = 50$  ns (e) for the microwave drive applied at  $\omega_{11 \rightarrow 21}$  to both qubits (solid lines) and selectively to qubit B only (dashed lines).

selectively to qubit B ( $\eta_A = 0$ ). This results in a gate similar to the cross-resonance scheme [4, 30]. We notice that certain matrix elements  $n_{kl \rightarrow k'l'}^\alpha$  remain equally zero for  $\hat{V} \neq 0$ . All two-qubit levels  $|kl\rangle$  can be separated into two families depending on the parity of  $k+l$ . To higher orders,  $\hat{V}$  mixes only levels with the same parity of  $k+l$ , while  $\hat{n}_\alpha$  only connects levels with different parities of  $k+l$ . We have  $n_{10 \rightarrow 12}^\alpha = 0$  when  $J_C \neq 0$ , while  $n_{10 \rightarrow 02}^B \neq 0$ .

To model the gate operation, we find the evolution operator  $\hat{U}(t)$  by integrating numerically  $i\hbar\partial\hat{U}(t)/\partial t = \hat{H}\hat{U}(t)$ . For a desired gate time  $t_g$ , we consider a Gaussian envelope  $f(t) = A\{\exp[-8t(t-t_g)/t_g^2] - 1\}$ , where we later optimize over  $A$  and the drive frequency  $\omega_d$  within 15 MHz window around  $\omega_{11 \rightarrow 21}$ . The evolution operator in the two-qubit computational subspace is represented by a non-unitary  $4 \times 4$  matrix  $\hat{U}_c$  defined by its matrix elements  $[\hat{U}_c]_{kl, k'l'} = \langle kl|\hat{U}(t_g)|k'l'\rangle$ , where  $|kl\rangle, |k'l'\rangle \in \{|00\rangle, |01\rangle, |10\rangle, |11\rangle\}$ . To compare  $\hat{U}_c$  with the ideal operator  $\hat{U}_{\text{CZ}}$ , we apply two instant single-qubit Z-rotations to get  $\hat{U}'_c = \hat{U}_Z\hat{U}_c$ , where  $\hat{U}_Z = \text{diag}[1, e^{i\delta\phi_{01}}, e^{i\delta\phi_{10}}, e^{i\delta\phi_{01}+i\delta\phi_{10}}]$ ,  $\delta\phi_{kl} = \phi_{kl} - \phi_{00}$ , and

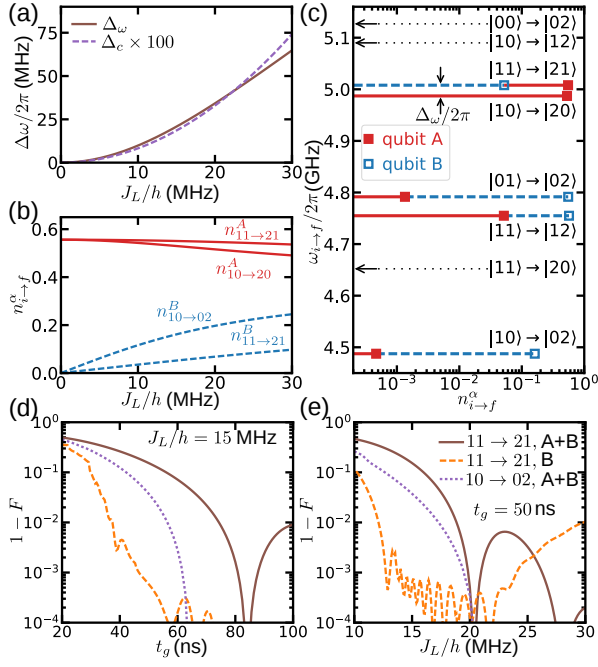


FIG. 3. (Color online) Numerical results for the inductive coupling. The notation follows Fig. 2 with  $J_C$  replaced by  $J_L$ . The results of panels (c) and (d) are for  $J_L/h = 15$  MHz. In addition, in panels (d) and (e), dotted lines show the results for the drive applied to both qubits at  $\omega_{10 \rightarrow 02}$ .

$\phi_{kl} = -\arg\{\hat{U}_c\}_{kl,kl}$ . We then calculate the averaged gate fidelity  $F = [\text{Tr}(\hat{U}_c^\dagger \hat{U}'_c) + |\text{Tr}(\hat{U}_{CZ}^\dagger \hat{U}'_c)|^2]/20$  [28, 31].

The gate error  $1 - F$  is shown in Figs. 2(d) and 2(e) as a function of  $t_g$  and  $J_C$  for the microwave drive applied to both qubits ( $\eta_A = \eta_B = 1$ , solid lines, as a worst-case scenario without local microwave control lines for each qubit), and selectively to qubit B ( $\eta_A = 0, \eta_B = 1$ , dashed lines). The gate error is lower in the second case. When the drive is applied to both qubits,  $J_C/h$  has to be  $\gtrsim 200$  MHz to achieve the 99% fidelity threshold within  $t_g = 100$  ns. For the selective drive of a single qubit, the same interaction strength of 200 MHz leads to the 99% fidelity for a shorter gate time of 50 ns, and the 99.9% fidelity is possible at  $t_g \approx 90$  ns. The 99.9% threshold can be achieved at  $t_g = 50$  ns for both designs provided  $J_C$  is sufficiently large. We expect that the gate error can be reduced further with more advanced microwave-pulse shaping [32].

*Inductive coupling* — For the coupling realized via a mutual inductance  $L_M \ll L_A, L_B$  as shown in Fig. 1(f), the interaction  $\hat{V}$  in Eq. (2) has the form

$$\hat{V} = -J_L \hat{\phi}_A \hat{\phi}_B \quad \text{with} \quad J_L = (\hbar/2e)^2 L_M / (L_A L_B), \quad (5)$$

and  $E_{L,\alpha}$  is the renormalized inductive energy.

The interaction effects within the computational subspace are important for inductive coupling. Nevertheless, this does not affect the phase accumulation rate  $\Delta_c$  since

nonzero contributions from repulsion between computational levels exactly cancel in  $\Delta_c$ . Moreover, similarly to the capacitive coupling,  $\Delta_c \ll \Delta_\omega$ , see Fig. 3(a), allowing for the same CZ gate by driving at  $\omega_{11 \rightarrow 21}$ . The frequency mismatch  $\Delta_\omega$  now occurs primarily because of the repulsion between  $|10\rangle_0$  and  $|01\rangle_0$  rather than  $|21\rangle_0$  and  $|12\rangle_0$ , see the wavy line in Fig. 1(g). This can be seen in the matrix elements in Fig. 3(b). There,  $n_{11 \rightarrow 21}^B$  does not grow as fast with the interaction strength as for the capacitive coupling, while  $n_{10 \rightarrow 20}^A$  decreases. The transition  $|10\rangle \rightarrow |02\rangle$  acquires a relatively large matrix element, allowing for another way of activating the CZ gate. Driving this transition can be advantageous since it can be better separated in frequency from other allowed transitions [Fig. 3(c)] for our choice of parameters. In this case, state  $|10\rangle$  changes sign, while other states are nearly unaffected, and an additional  $Z_\pi = \text{diag}(1, e^{i\pi})$  gate applied to qubit A will reduce the gate to its standard form  $\hat{U}_{CZ}$ .

We present gate errors for the inductive coupling in Figs. 3(d) and 3(e). If the selective single-qubit drive is not possible, then driving at  $\omega_{10 \rightarrow 02}$  is generally a better option than driving at  $\omega_{11 \rightarrow 21}$ . The selective drive at  $\omega_{11 \rightarrow 21}$  further reduces the gate error at a reasonably small interaction strength ( $J_L/h < 20$  MHz) or short gate time ( $t_g < 60$  ns). The nonmonotonic behavior in the gate fidelity [solid and dashed line in Fig. 3(e)] is explained by a decrease in separation between  $\omega_{01 \rightarrow 02}$  and  $\omega_{11 \rightarrow 21}$  with increasing  $J_L/h$  and a relatively large value of  $n_{01 \rightarrow 02}^B$ .

*Conclusion and outlook* — We have analyzed both inductive and capacitive interactions between two fluxoniums and found that gate fidelities of 99.9% are possible within 100 ns gate times. Capacitive coupling scheme may be easier to realize but will require controlling the drive amplitude at both qubits, similar to the operation of the cross-resonance gate [4, 30]. Inductive scheme is much less sensitive to cross-talks and state leakage but may require fine-tuning of single-qubit gates or tunable couplers [33]. Our work suggests that fluxonium qubits can be a potential upgrade to the mainstream transmons as building blocks for a large quantum information processor. While transmon qubits face the challenges of anharmonicity-limited gate speed and lifetime limited by surface material ( $T_1 < 100 \mu\text{s}$ ) [34], the fluxonium at half flux quantum has millisecond energy relaxation time [35] and no fundamental obstacles to achieve comparably long coherence time (the second-order flux noise at half-quantum bias is not yet a limiting factor [36]) together with sub-100 ns two-qubit gates.

The extraordinary lifetime of the fluxonium  $|0\rangle \rightarrow |1\rangle$  transition is partially enabled by nature of its very low (sub-GHz) frequency, which we believe is a virtue rather than a weakness for quantum computation. The energy relaxation rate due to dielectric loss is proportionally slower at low frequencies at a constant  $Q$ -factor (in fact,

$Q$  usually improves at lower frequencies [37]). Although fluxonium qubits will operate in a relatively “hot” environment due to their low qubit frequency, a practical quantum processor in any case will have to employ active qubit state initialization such as measurement feedback for either rapid reset or suppressing nonequilibrium excitations [38, 39]. The fidelity of the state initialization directly benefits from long  $T_1$ .

The proposed CZ gate is made possible by rich energy level structure of the fluxonium and separation of its well-protected memory space from strongly-interacting states. This concept is applicable to other anharmonic qubits with a hierarchy of transition matrix elements, such as variants of flux qubits [36]. In practice, the performance of the proposed CZ gate will depend on qubit coherence times and will likely be limited by the  $T_2$  time of the  $|2\rangle$  state, which is accessed during the gate. Because the  $\sim 5$  GHz  $|1\rangle \rightarrow |2\rangle$  transition is similar to transmon transitions, it should be possible to achieve  $T_2$  time on the order of 50  $\mu$ s with today’s technology [24], limiting incoherent error to less than 0.1%. Therefore, the CZ gate for fixed-frequency fluxonium qubits provides a quite promising pathway towards the long-coveted 99.9% fidelity two-qubit gates.

*Acknowledgements* — We would like to thank Robert McDermott, Long Nguyen, Mark Saffman, and Zhenyi Qi for fruitful discussions.

- 
- [1] J. Koch, T. M. Yu, J. Gambetta, A. A. Houck, D. I. Schuster, J. Majer, A. Blais, M. H. Devoret, S. M. Girvin, and R. J. Schoelkopf, *Phys. Rev. A* **76**, 042319 (2007).
- [2] M. H. Devoret and R. J. Schoelkopf, *Science* **339**, 1169 (2013).
- [3] C. Rigetti, J. M. Gambetta, S. Poletto, B. L. T. Plourde, J. M. Chow, A. D. Córcoles, J. A. Smolin, S. T. Merkel, J. R. Rozen, G. A. Keefe, M. B. Rothwell, M. B. Ketchen, and M. Steffen, *Phys. Rev. B* **86**, 100506 (2012).
- [4] S. Sheldon, E. Magesan, J. M. Chow, and J. M. Gambetta, *Phys. Rev. A* **93**, 060302 (2016).
- [5] J. M. Chow, J. M. Gambetta, L. Tornberg, J. Koch, L. S. Bishop, A. A. Houck, B. R. Johnson, L. Frunzio, S. M. Girvin, and R. J. Schoelkopf, *Phys. Rev. Lett.* **102**, 090502 (2009).
- [6] A. A. Houck, J. A. Schreier, B. R. Johnson, J. M. Chow, J. Koch, J. M. Gambetta, D. I. Schuster, L. Frunzio, M. H. Devoret, S. M. Girvin, and R. J. Schoelkopf, *Phys. Rev. Lett.* **101**, 080502 (2008).
- [7] P. Campagne-Ibarcq, E. Flurin, N. Roch, D. Darson, P. Morfin, M. Mirrahimi, M. H. Devoret, F. Mallet, and B. Huard, *Phys. Rev. X* **3**, 021008 (2013).
- [8] M. Hatridge, S. Shankar, M. Mirrahimi, F. Schackert, K. Geerlings, T. Brecht, K. M. Sliwa, B. Abdo, L. Frunzio, S. M. Girvin, R. J. Schoelkopf, and M. H. Devoret, *Science* **339**, 178 (2013).
- [9] M. Takita, A. D. Córcoles, E. Magesan, B. Abdo, M. Brink, A. Cross, J. M. Chow, and J. M. Gambetta, *Phys. Rev. Lett.* **117**, 210505 (2016).
- [10] C. Neill, P. Roushan, K. Kechedzhi, S. Boixo, S. V. Isakov, V. Smelyanskiy, R. Barends, B. Burkett, Y. Chen, Z. Chen, B. Chiaro, A. Dunsworth, A. Fowler, B. Foxen, R. Graff, E. Jeffrey, J. Kelly, E. Lucero, A. Megrant, J. Mutus, M. Neeley, C. Quintana, D. Sank, A. Vainsencher, J. Wenner, T. C. White, H. Neven, and J. M. Martinis, arXiv:1709.06678 (2017).
- [11] C. Song, K. Xu, W. Liu, C.-p. Yang, S.-B. Zheng, H. Deng, Q. Xie, K. Huang, Q. Guo, L. Zhang, P. Zhang, D. Xu, D. Zheng, X. Zhu, H. Wang, Y.-A. Chen, C.-Y. Lu, S. Han, and J.-W. Pan, *Phys. Rev. Lett.* **119**, 180511 (2017).
- [12] L. DiCarlo, J. M. Chow, J. M. Gambetta, L. S. Bishop, B. R. Johnson, D. I. Schuster, J. Majer, A. Blais, L. Frunzio, S. M. Girvin, and R. J. Schoelkopf, *Nature* **460**, 240 (2009).
- [13] D. C. McKay, S. Filipp, A. Mezzacapo, E. Magesan, J. M. Chow, and J. M. Gambetta, *Phys. Rev. Applied* **6**, 064007 (2016).
- [14] H. Paik, A. Mezzacapo, M. Sandberg, D. T. McClure, B. Abdo, A. D. Córcoles, O. Dial, D. F. Bogorin, B. L. T. Plourde, M. Steffen, A. W. Cross, J. M. Gambetta, and J. M. Chow, *Phys. Rev. Lett.* **117**, 250502 (2016).
- [15] M. V. G. Dutt, L. Childress, L. Jiang, E. Togan, J. Maze, F. Jelezko, A. S. Zibrov, P. R. Hemmer, and M. D. Lukin, *Science* **316**, 1312 (2007).
- [16] G. Vittorini, D. Hucul, I. V. Inlek, C. Crocker, and C. Monroe, *Phys. Rev. A* **90**, 040302 (2014).
- [17] K. M. Maller, M. T. Lichtman, T. Xia, Y. Sun, M. J. Piotrowicz, A. W. Carr, L. Isenhower, and M. Saffman, *Phys. Rev. A* **92**, 022336 (2015).
- [18] M. Mariantoni, H. Wang, T. Yamamoto, M. Neeley, R. C. Bialczak, Y. Chen, M. Lenander, E. Lucero, A. D. O’Connell, D. Sank, M. Weides, J. Wenner, Y. Yin, J. Zhao, A. N. Korotkov, A. N. Cleland, and J. M. Martinis, *Science* **334**, 61 (2011).
- [19] S. Rosenblum, Y. Y. Gao, P. Reinhold, C. Wang, C. J. Axline, L. Frunzio, S. M. Girvin, L. Jiang, M. Mirrahimi, M. H. Devoret, and R. J. Schoelkopf, arXiv:1709.05425 (2017).
- [20] V. E. Manucharyan, J. Koch, L. I. Glazman, and M. H. Devoret, *Science* **326**, 113 (2009).
- [21] V. E. Manucharyan, N. A. Masluk, A. Kamal, J. Koch, L. I. Glazman, and M. H. Devoret, *Phys. Rev. B* **85**, 024521 (2012).
- [22] Y.-H. Lin, L. B. Nguyen, N. Grabon, J. S. Miguel, N. Pankratova, and V. E. Manucharyan, arXiv:1705.07873 (2017).
- [23] J. Koch, V. Manucharyan, M. H. Devoret, and L. I. Glazman, *Phys. Rev. Lett.* **103**, 217004 (2009).
- [24] V. E. Manucharyan, in preparation (2018).
- [25] G. Zhu and J. Koch, *Phys. Rev. B* **87**, 144518 (2013).
- [26] G. Zhu, D. G. Ferguson, V. E. Manucharyan, and J. Koch, *Phys. Rev. B* **87**, 024510 (2013).
- [27] U. Vool and M. Devoret, *Int. J. Circ. Theor. Appl.* **45**, 897 (2017).
- [28] J. Ghosh, A. Galiutdinov, Z. Zhou, A. N. Korotkov, J. M. Martinis, and M. R. Geller, *Phys. Rev. A* **87**, 022309 (2013).
- [29] J. M. Chow, J. M. Gambetta, A. W. Cross, S. T. Merkel, C. Rigetti, and M. Steffen, *New J. Phys.* **15**, 115012 (2013).
- [30] J. M. Chow, A. D. Córcoles, J. M. Gambetta, C. Rigetti, B. R. Johnson, J. A. Smolin, J. R. Rozen, G. A. Keefe,

- M. B. Rothwell, M. B. Ketchen, and M. Steffen, *Phys. Rev. Lett.* **107**, 080502 (2011).
- [31] L. H. Pedersen, N. M. Møller, and K. Mølmer, *Phys. Lett. A* **367**, 47 (2007).
- [32] F. Motzoi, J. M. Gambetta, P. Rebentrost, and F. K. Wilhelm, *Phys. Rev. Lett.* **103**, 110501 (2009).
- [33] Y. Chen, C. Neill, P. Roushan, N. Leung, M. Fang, R. Barends, J. Kelly, B. Campbell, Z. Chen, B. Chiaro, A. Dunsworth, E. Jeffrey, A. Megrant, J. Y. Mutus, P. J. J. O'Malley, C. M. Quintana, D. Sank, A. Vainsencher, J. Wenner, T. C. White, M. R. Geller, A. N. Cleland, and J. M. Martinis, *Phys. Rev. Lett.* **113**, 220502 (2014).
- [34] C. Wang, C. Axline, Y. Y. Gao, T. Brecht, Y. Chu, L. Frunzio, M. H. Devoret, and R. J. Schoelkopf, *Appl. Phys. Lett.* **107**, 162601 (2015).
- [35] I. M. Pop, K. Geerlings, G. Catelani, R. J. Schoelkopf, L. I. Glazman, and M. H. Devoret, *Nature* **508**, 369372 (2014).
- [36] F. Yan, S. Gustavsson, A. Kamal, J. Birenbaum, A. P. Sears, D. Hover, T. J. Gudmundsen, D. Rosenberg, G. Samach, S. Weber, J. L. Yoder, T. P. Orlando, J. Clarke, A. J. Kerman, and W. D. Oliver, *Nature Comm.* **7**, 12964 (2016).
- [37] V. Braginsky, V. Ilchenko, and K. Bagdassarov, *Phys. Lett. A* **120**, 300 (1987).
- [38] D. Ristè, C. C. Bultink, K. W. Lehnert, and L. DiCarlo, *Phys. Rev. Lett.* **109**, 240502 (2012).
- [39] P. Magnard, P. Kurpiers, B. Royer, T. Walter, J.-C. Besse, S. Gasparinetti, M. Pechal, J. Heinsoo, S. Storz, A. Blais, and A. Wallraff, arXiv:1801.07689 (2018).